Absence of a multiglass state in some transition metal doped quantum paraelectrics

Charu Garg,[1] Jitender Kumar,[1] and Sunil Nair[1,2]

[1]*Department of Physics, Indian Institute of Science Education and Research, Dr. Homi Bhabha Road, Pune, Maharashtra-411008, India*
[2]*Centre for Energy Science, Indian Institute of Science Education and Research, Dr. Homi Bhabha Road, Pune, Maharashtra-411008, India*

We critically investigate the purported existence of a multiglass state in the quantum paraelectrics $SrTiO_3$ and $KTaO_3$ doped with magnetic $3d$ transition metals. We observe that the transition metals have limited solubility in these hosts, and that traces of impurity magnetic oxides persist even in the most well-processed specimens. Our dielectric measurements indicate that the polar nanoregions formed as a consequence of doping appear to lack co-operativity, and the associated relaxation process exhibits a thermally activated Arrhenius form. At lower temperatures, the dielectric susceptibility could be fit using the Barrett's formalism, indicating that the quantum-paraelectric nature of the host lattices is unaltered by the doping of magnetic transition metal oxides. All these doped quantum paraelectrics exhibit a crossover from the high-temperature Curie-Weiss regime to one dominated by quantum fluctuations, as evidenced by a T^2 dependence of the temperature-dependent dielectric susceptibility. The temperature dependence of the magnetic susceptibility indicates that magnetic signatures observed in some of the specimens could be solely ascribed to the presence of impurity oxides corresponding to the magnetic dopants used. Hence, the doped quantum paraelectrics appear to remain intrinsically paramagnetic down to the lowest measured temperatures, ruling out the presence of a multiglass state.

I. INTRODUCTION

Multiferroics—materials with coexisting magnetic and polar orders—have been at the forefront of extensive theoretical and experimental investigations. Initially thought to be phenomena that are inimical to each other, a variety of avenues are now known, by which a system can be tailored to exhibit both of these orders [1]. Not surprisingly, advances in this area of research have been fuelled by the continuous availability of new materials, which exhibit coupling between electric and magnetic order parameters. Multiferroics can be broadly divided into two different classes: type-I multiferroics, where magnetic and polar orders arise from independent microscopic origins, and type-II multiferroics, where a nontrivial magnetic order facilitates ferroelectricity [2,3]. An additional variant has also been reported—that in which both the magnetic and polar orders are frozen and these *multiglasses* are purported to be characterized by the coexistence of a magnetic spin/cluster glass with a polar cluster glass phase [4,5].

The genesis of the area of multiglasses can be traced to the report of the simultaneous occurrence of a nonergodic polar and magnetic glass state in the doped quantum paraelectric $Sr_{0.98}Mn_{0.02}TiO_3$ [6,7]. It was suggested that the Mn^{2+} ions that replace the Sr^{2+} species in $SrTiO_3$ undergo off-center displacements from their mean positions, creating electric dipoles. Such polar clusters then undergo a low-temperature transition to a frozen relaxor-like state at $T_G = 38$ K as was evidenced by a power-law dependence of the frequency-dependent dielectric susceptibility [6]. Since Mn^{2+} is also magnetic ($S = 5/2$), they couple to each other via frustrated antiferromagnetic superexchange interactions, and below T_G the freezing of polar clusters also triggers the freezing of

spin degrees of freedom. This effect is also augmented by the presence of a finite magnetoelectric coupling, which couples the polar and spin degrees of freedom, resulting in a *magnetoelectric multiglass* state in $Sr_{0.98}Mn_{0.02}TiO_3$. Though the closely related $K_{0.97}Mn_{0.03}TaO_3$ system was also reported to harbor such a state [8], it was later described as a spin cluster glass where the interacting polar clusters fail to condense into a glassy state [9]. The coexistence of magnetic and polar glasslike states was also reported in the double perovskite La_2NiMnO_6 [10] and the delafossite $CuCr_{0.5}V_{0.5}O_2$ [11] systems, with the antisite disorder (between the Ni-Mn and Cr-V species, respectively) being responsible for the observed multiglass state.

A number of experimental signatures were used to characterize this multiglass state in $Sr_{0.98}Mn_{0.02}TiO_3$ [4,5]. These included (i) magnetic irreversibility in the zero-field-cooled and field-cooled measuring protocols, (ii) the observation of a frequency-dependent ac susceptibility that appears to coincide with the polar freezing temperature, (iii) a power-law fit to the peak temperature of the real part of the dielectric permittivity $\epsilon'(T)$, (iv) memory effects in both the polar and magnetic sectors, and (v) a peak in the nonlinear dielectric susceptibility [6–8].

However, there have been a number of subsequent reports that have raised doubts about the validity of the multiglass scenario in this system [12], and in the transition metal doped quantum paraelectrics in general. The significant observations that are not commensurate with the existence of a multiglass state included (i) the absence of magnetic freezing in specimens synthesized using different synthesis procedures such as high-energy ball milling [13] and the oxalate precipitate method [14], and (ii) transmission electron micrographs

indicating that the magnetic anomaly was only observed in those specimens where a network of structural defects was present [13]. The inference therein was that the existence of structural defects was an indicator of the fact that the dopant (Mn) was not homogeneously distributed in the host lattice, and that the segregation of these magnetic dopants (and possibly their oxides) was responsible for the observed magnetic signatures. (iii) Investigations were performed with careful site-specific Mn substitutions indicating that $Sr_{0.98}Mn_{0.02}TiO_3$ does not exhibit any magnetic ordering/anomalies, whereas Mn codoped in both the Sr and Ti sites exhibits glassy magnetic properties of extrinsic origin [12]. Doping the sample at the Ti site left the system in a paraelectric state, whereas doping at the Sr (and Sr and Ti simultaneously) site led to the formation of a relaxor-like state. The magnetic ordering was proven to be decoupled from the dielectric one, thus ruling out the possibility of a multiglass phase in these systems. Moreover, it was explicitly stated that the magnetic anomaly observed in the Sr- and Ti-site codoped Mn was due to the presence of Mn_3O_4 impurities in small quantities. Finally, (iv) there was no frequency dependence in the measured nonlinear dielectric susceptibility [8].

The main point of contention pertained to freezing in the magnetic sector, and the possibility that the observed glassy magnetic signatures arise from a small amount of the spinel Mn_3O_4, which is reported to exhibit a ferrimagnetic transition at ≈ 43 K [10,13]. At the small doping percentages under consideration here, these trace impurities are not easily discernible from routine x-ray diffraction measurements. This problem is accentuated by the fact that Mn_3O_4 can dissolve small amounts of TiO_2 (which is typically used as a raw material in the synthesis of $Sr_{0.98}Mn_{0.02}TiO_3$) [13], and it could also exhibit finite-size effects when it exists in the form of small impurity clusters within the perovskite matrix, thus exhibiting a sample-dependent variation of the observed (glasslike) magnetic transition temperature. The pristine Mn_3O_4 phase is also reported to be a magnetodielectric, which exhibits a number of closely spaced spin reorientation transitions with clear dielectric anomalies corresponding to these different transitions [15,16].

The fact that Mn_3O_4 exhibits a phase transition in close proximity to the energy scale of the relaxor state in these doped quantum paraelectrics should mean that this ambiguity should be unique to Mn doping alone. Other magnetic transition metal dopants (Co, Fe, or Ni) could offer a means of evaluating the existence of a multiglass state in the doped quantum paraelectrics, since the transition temperatures associated with the possible trace impurities (CoO, Co_3O_4, Fe_2O_3, Fe_3O_4, NiO, or Ni_2O_3) are very different from the temperature range of interest here. However, to the best of our knowledge there has been no attempt to evaluate the feasibility of a magnetically frozen state in quantum paraelectrics doped with different magnetic transition metal dopants. Here, we report an investigation of specimens of $Sr_{0.98}M_{0.02}TiO_3$ (SMT) and $K_{0.97}M_{0.03}TaO_3$ (KMT), with $M =$ Mn, Co, Fe, or Ni, synthesized using the solid-state ceramic route. These samples are characterized using x-ray diffraction, energy-dispersive x-ray analysis, and temperature dependent dielectric and magnetization measurements. Though all the doped specimens exhibit frequency-dependent features in the dielectric loss, our data

do not indicate the presence of a frozen polar state in any of these systems. Moreover, all the observed magnetic signatures can be clearly attributed to arising from the presence of oxides of the magnetic dopants used. Thus, our observations suggest that transition metal doped quantum paraelectrics clearly do not harbor an intrinsic glassy state in either the polar or the magnetic sectors.

II. EXPERIMENT

Polycrystalline specimens of the $Sr_{0.98}M_{0.02}TiO_3$ and $K_{0.97}M_{0.03}TaO_3$ series were synthesized by the standard solid-state reaction technique. For the SMT series, stoichiometric amounts of the preheated reagents were treated twice at 1150 °C followed by pelletizing and a final treatment at 1500 °C for 24 h. For the KMT series, the protocol was slightly different, and stoichiometric amounts of the preheated reagents were mixed and ground thoroughly in a glove box for 3 h, followed by a heat treatment at 1000 °C. This mixture was then reground and pelletized before being subjected to a final heat treatment at 1000 °C for 24 h. Multiple batches of samples were synthesized, and only the best ones were used for further investigations.

The phase purity of all the specimens was confirmed by x-ray powder diffraction (XRD) patterns, measured using a Bruker D8 Advance diffractometer with a Cu $K\alpha$ source. Elemental compositions were reconfirmed by using an energy-dispersive x-ray spectrometer (Ziess Ultra Plus). Magnetization measurements were performed using a Quantum Design (MPMS-XL) SQUID magnetometer. Temperature-dependent dielectric measurements were performed in the standard parallel plate geometry, using a NOVOCONTROL (Alpha-A) High Performance Frequency Analyzer. Measurements were typically done using an excitation ac signal of 1 V at frequencies varying from 1 kHz to 0.5 MHz.

III. RESULTS AND DISCUSSIONS

A. XRD analysis

The $SrTiO_3$ and $KTaO_3$ specimens stabilize in the cubic symmetry (space group *Pm-3m*), and doping by these percentages (2% and 3% in the SMT and KMT series, respectively) only results in very small changes in the lattice parameters, with no change in the crystallographic symmetry. Here it is critical to evaluate if the XRD patterns reveal the precipitation of any of the doped transition metal oxides in the form of impurity phases. Figure 1 shows the normalized XRD patterns for all the doped SMT and KMT compounds. The 2θ range depicted here encompasses the values corresponding to the highest intensity peaks of the transition metal oxides (Co_2O_3, CoO, Co_3O_4, Fe_2O_3, Fe_3O_4, MnO_2, Mn_2O_3, Mn_3O_4, NiO, or Ni_2O_3) possible as a result of Co, Fe, Mn, or Ni doping. Though impurity phase detection with such small amounts of doping is typically difficult with routine XRD measurements, we have tried to glean as much information as possible by using long counting times (of the order of 6–8 h) in these selected 2θ ranges. In the case of the SMT series, all the doped specimens were seen to be phase-pure, and no traces of any impurity oxides could be inferred from our XRD measurements. In the KMT series, the Co [Fig. 1(a)] and the
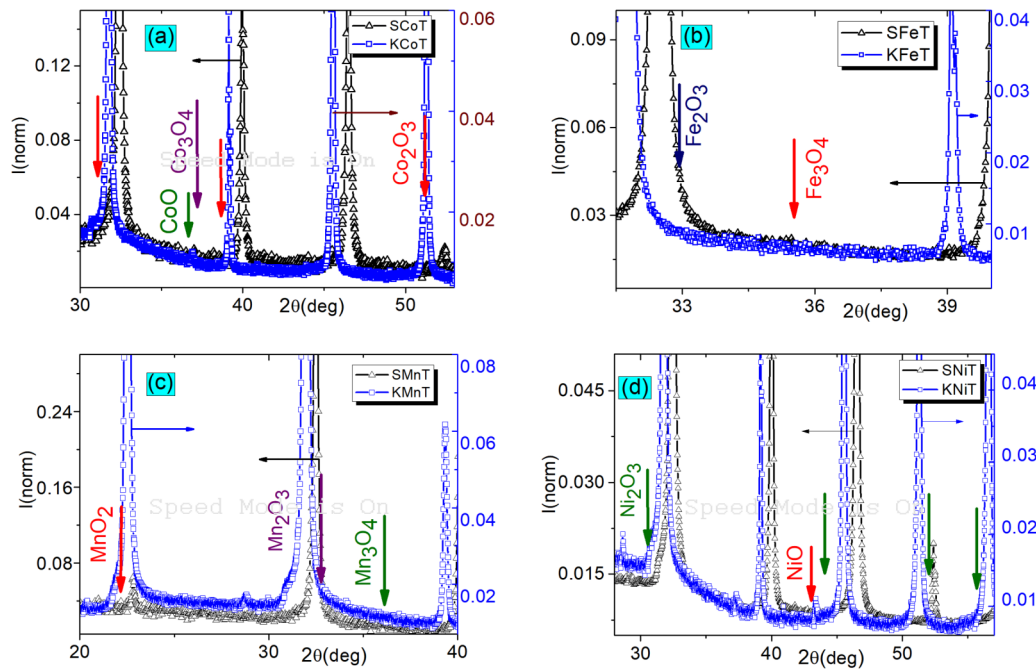
FIG. 1. Room-temperature x-ray diffraction data of the $KTaO_3$ and $SrTiO_3$ specimens doped with (a) Co, (b) Fe, (c) Mn, and (d) Ni. The 2θ ranges have been selected such that it encompasses the region where the most intense peak of the possible magnetic impurities (if any) can be clearly seen.

Ni [Fig. 1(d)] doped specimens appear to show faint traces corresponding to the Co_3O_4 and NiO phases, with the Fe- and Mn-doped specimens [Figs. 1(b) and 1(c)] being completely free from any spurious phases.

Scanning electron microscopy (SEM) and energy-dispersive x-ray spectroscopy (EDS) measurements were done on pellets of all the specimens of the SMT and KMT series (20 KV) for microstructural analysis. Figure 2 depicts the micrographs for the SMT specimens, all of which show arbitrarily shaped grains with reasonably large size distribution. Since the dopant percentage is very low, EDS was performed at more than two dozen areas in each specimen. Though the percentage of dopants deduced from the EDS measurements is consistent with the doping values, we observed a lower percentage of Ti in some cases. This is possibly because A site substitution in $SrTiO_3$ is not completely site-selective. It has been reported, at least for the case of Mn, that it continues to partially occupy the Ti site irrespective of the synthesis protocol used [17]. For this reason, the solid solubility limit of Mn in the Sr site of $SrTiO_3$ site has never been properly determined. Though similar studies are lacking for the other transition metals used in this study, our EDS investigations indicate that this problem appears to be generic to all the transition metals used in this investigation.

In the case of the KMT series (Fig. 3), we observe uniform cubelike microstructure, and the grains appear to have a much narrower size distribution, with clean rectangular facets and no evidence of any kind of phase clustering. The results of EDS measurements indicate no observable deviation from the actual doping percentages, suggesting that the transition metals appear to be fully incorporated in the lattice. How-ever, considering the fact that long XRD scans suggested

the possibility of spurious Co_3O_4 and NiO phases, and that the solubility limit of these dopants in the $KTaO_3$ lattice is questionable, we performed additional backscattered scans on all these specimens. With the backscattering coefficient being a function of the atomic number, the contrast observed in backscattered images is known to offer a means of identifying regions of compositional inhomogeneities [18].
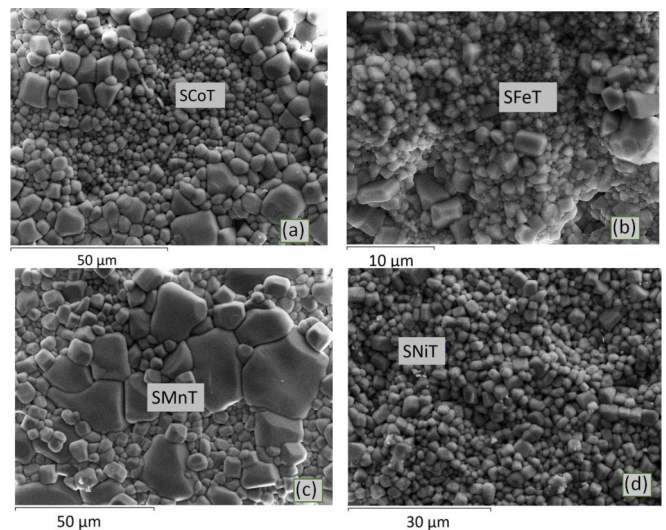

FIG. 2. Scanning electron micrographs of $SrTiO_3$ specimens doped with (a) Co, (b) Fe, (c) Mn, and (d) Ni. Note that all the scans were performed on the piece of a pellet that gets manifested in the form of high density and homogeneity of grains. Scans were performed on various regions of the pellet, and the obtained elemental contribution was consistent with the expected ratio.
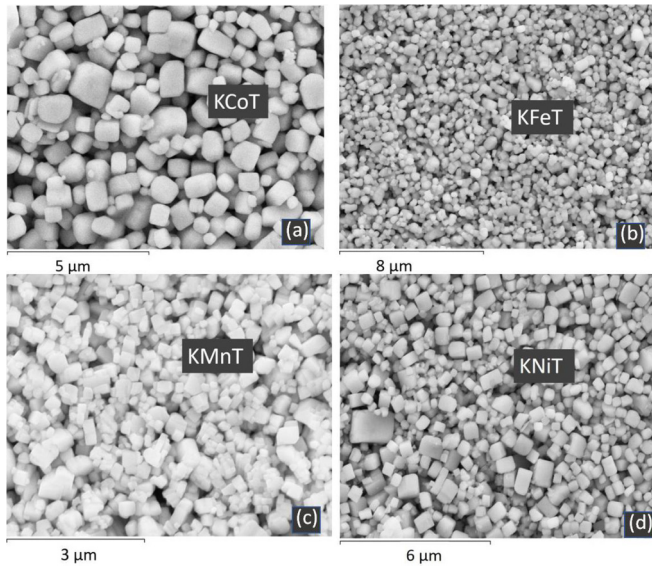
FIG. 3. Scanning electron micrographs of the KTaO$_3$ specimens doped with (a) Co, (b) Fe, (c) Mn, and (d) Ni. The sample is highly homogeneous and shows distinctly ordered cubic structure down to a few μm. All the scans were performed on a piece of pellet and showed great overlap with the expected stoichiometry of the elements.

FIG. 4. Backscattered images of the KTaO$_3$ specimens doped with (a) Co, (b) Fe, (c) Mn, and (d) Ni. Selected regions (in the center) that exhibited an intensity contrast corresponding to possible chemical inhomogeneities are depicted. These dark regions depicts the segregation of the transition metal oxide by exhibiting high concentration values of the respective transition metal oxide when scanned within this region, implying segregation of dopant oxides.

After carefully sampling close to two dozen locations in the backscattering mode, we observed regions where traces of the dopant oxides Mn$_3$O$_4$, Co$_3$O$_4$, and Fe$_2$O$_3$ were seen. Identifying traces of NiO was even more difficult, and such regions could only be identified after extensive scanning. These images, where the trace impurities are evident in the form of an image contrast, are depicted in Fig. 4. Our exhaustive EDS measurements indicate that the solubility limit of the transition metal dopants varies from one host to the other, and also on the transition metal used. Considering the problem one is trying to address, our observations indicate that a combination of XRD and normal and backscattering EDS measurements is imperative in evaluating the phase purity of these systems. Our observations also indicate that all these magnetic transition metal elements have limited solubility in the SrTiO$_3$ and KTaO$_3$ lattices, and use of x-ray diffraction alone is not adequate to highlight the phase purity of such systems. Though not included as a part of our study, high-resolution synchrotron measurements could be more effective in identifying the presence of impurity phases as compared to long waiting times in laboratory x-ray diffraction. Additional information could also probably be obtained by using resonant x-ray scattering measurements.

B. Dielectric analysis

SrTiO$_3$ and KTaO$_3$ are both known to be polarizable soft ferroelectric hosts, and the off-centered shifts of the M^{2+} ions when doped at the 12-fold coordinated Sr or K positions is thought to induce electrical dipoles. These dipoles then condense in the form of polar nanoclusters, the dynamics of which can be discerned using dielectric spectroscopy measurements. Figure 5 summarizes the frequency-dependent measurements
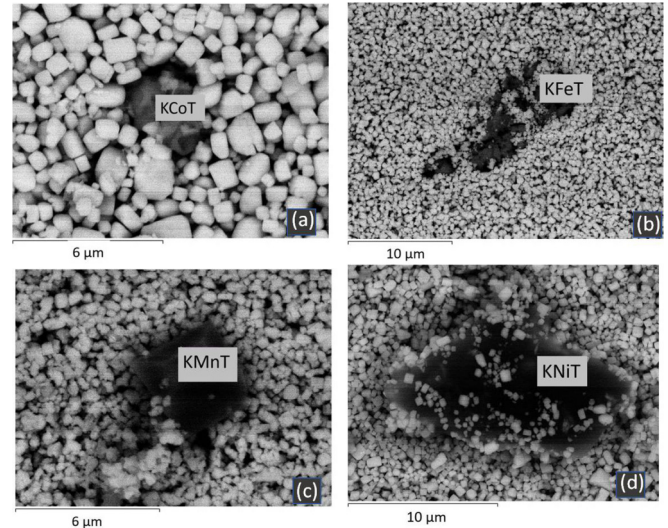
of the real part of the dielectric susceptibility [$\epsilon'(T)$] over a broad temperature range for both the KMT and SMT series (inset). All the specimens exhibit a pronounced increase in $\epsilon'(T)$ as a function of decreasing temperature, as is the norm for quantum paraelectrics. We note that in pristine KTaO$_3$, a peak in the loss tangent and an anomaly in the real part of the permittivity have been reported earlier [19,20], presumably arising as a consequence of defect dipoles. The influence of the polar regions formed as a consequence of our transition metal doping is more clearly evident in the temperature-dependent scans of the imaginary component of the dielectric susceptibility [$\epsilon''(T)$], as is shown in Fig. 6, where SrTiO$_3$ doped with (a) Co, (b) Fe, (c) Mn, and (d) Ni is depicted in the left panel, and KTaO$_3$ doped with (e) Co, (f) Fe, (g) Mn, and (h) Ni is depicted in the right one. A broad frequency-dependent peak is observed in all the specimens, with the peak in $\epsilon''(T)$ shifting to higher temperatures with increasing frequency. This is a signature of soft ferroelectric hosts, and it reflects the dynamics of polar domains that form as a consequence of transition metal doping. The size/volume distribution of these domains is typically dependent on both the synthesis conditions as well as the nature of the dopant, as is reflected in subtle differences in both the peak position as well as its frequency dependence between the different specimens. The dynamics associated with these polar regions are not easily seen in the real part of the dielectric susceptibility $\epsilon'(T)$ due to its dramatic increase at low temperatures, associated with the renormalization of the soft-mode frequency, with this increase being three orders of magnitude larger than that observed in $\epsilon''(T)$. The thermodynamic fluctuations associated with the different dopants results in an effective softening (or hardening) of this mode and dictates the effective values of $\epsilon(T)$ attained at low temperatures.
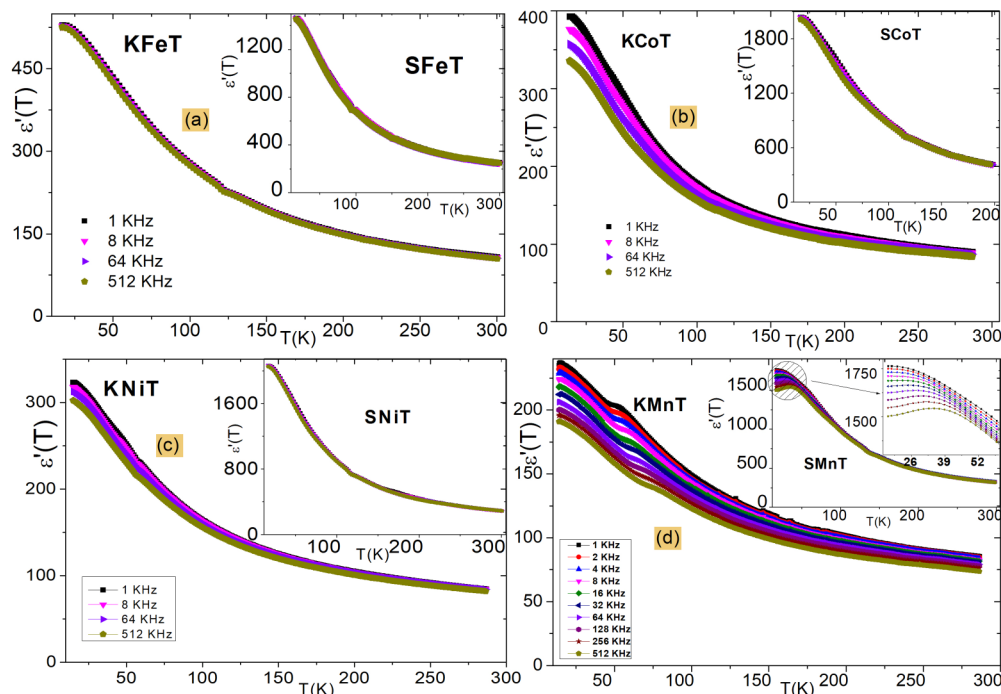
FIG. 5. Temperature dependence of the real part of the dielectric susceptibility as measured at different probing frequencies for the doped SrTiO$_3$ (insets) and doped KTaO$_3$ [main panels (a), (b), (c), and (d)] specimens. Only the Mn-doped specimens (d) appear to exhibit an appreciable frequency dependence.

The frequency-dependent relaxation peaks observed in the temperature-dependent imaginary permittivity can be analyzed to shed light on the processes responsible for the observed relaxation. The symmetry of the perovskite lattices, in our case SMT and KMT, allows it to hold several equivalent orientations for the dipoles formed due to disorder induced via doping. If these dipoles interact strongly and freezes into a glasslike state upon lowering the temperature, one would expect to see signatures of a dynamical slowing down, which is described by a VFT formalism given as $f = f_0 \exp \frac{-E}{k_b[T-T_G]}$, where f_0, E, and T_G correspond to the jump attempt frequency, the energy barrier associated with this process, and the temperature of the glass transition below which the dynamics are frozen in perspective with our measurement time scales. In contrast, if the dipoles lack cooperativity, the dipoles can hop among these equivalent orientations as a consequence of thermal activation. In this case, $T_G \to 0$ K, and the VFT equation is modified to a thermally activated Arrhenius form given by $f = f_0 \exp \frac{-E}{k_b T}$. We attempted to fit the observed relaxation process to the VFT, power law, and Arrhenius forms, and we observed that best fits in all cases are given by the Arrhenius equation. This is shown in Fig. 7 for all the members of the KMT (top) and SMT (bottom) series. This indicates that the density of dipoles formed by the doping of transition metal ions in the STO and KTO hosts is quite small for the doping percentages used in our investigations, and that the interaction between these dipoles is not strong enough to achieve collective freezing. There appears to be a trend in the deduced activation energies (Table I), as we see that $E_{Co} < E_{Ni} < E_{Mn}$ for both families. Interestingly, Fe doping exhibits very different values for both series, as the value of E_{Fe} is maximum in the SMT specimens and the lowest in the KMT ones. This could presumably arise due to a substantial difference in the solubility limit of Fe in both systems.

In doped quantum paraelectrics, the deviations from Curie-Weiss behavior seen at low temperatures are typically ascribed to the influence of quantum fluctuations. The observed functional form has been described by Barrett's equation $\epsilon'(T) = A + C/[(T_1/2)\coth(T_1/2T) - T_0]$, where A is a fitting constant [often ignored when the values of $\epsilon'(T, f)$ are sufficiently large], C is the Curie constant, T_0 is equivalent to the classical Curie temperature, and T_1 represents the temperature below which quantum fluctuations overwhelm the thermal ones [21]. As is shown in Fig. 8, good fits to Barrett's equation were obtained for the $\epsilon'(T)$ data for the Ni, Co, and Fe specimens of both the SMT (top) and KMT (bottom) series, reinforcing our observation regarding the absence of a relaxor state. The fits to the dielectric susceptibility data of the Mn-doped specimens of both series are depicted in the insets of Fig. 8. This indicates that the dielectric behavior of the Mn-doped specimens is distinct from those of the other transition metal doped members. This is also in broad agreement with an earlier report in which the dielectric properties of the Mn-doped KTaO$_3$ were suggested to be different from its Fe doped analog [22]. There, it was reported that whereas the Mn-doped specimen depicted a peaklike anomaly in $\epsilon'(T)$, the Fe-doped analog did not exhibit this feature and retained a quantum paraelectric-like behavior down to the lowest measured temperatures. Pressure- and temperature-dependent dielectric measurements were also used to suggest that the Mn doping induced dipolar entities appear to couple more strongly to the soft mode of the host quantum paraelectric lattice.
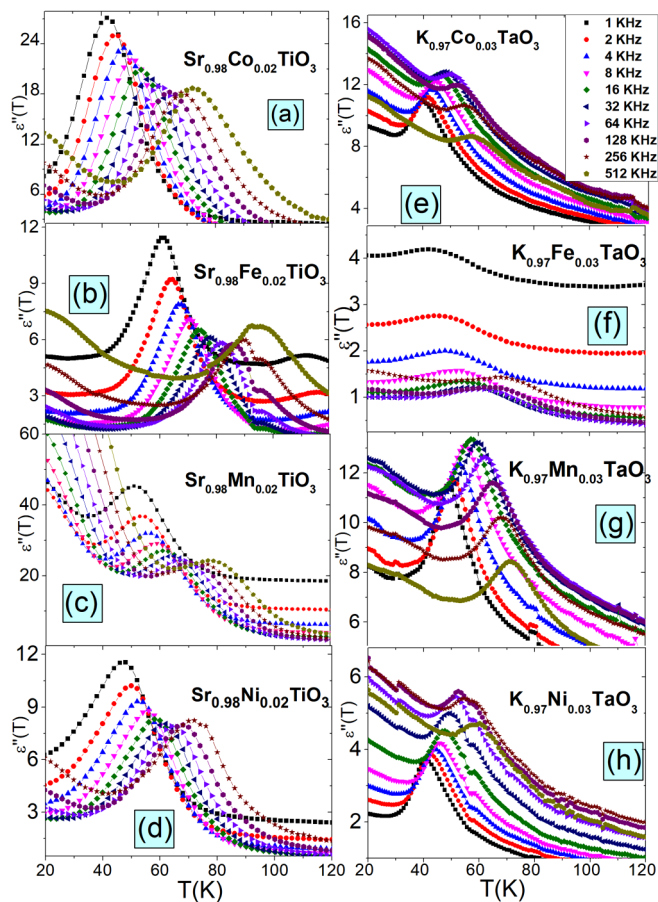
FIG. 6. Temperature dependence of the imaginary part of the dielectric susceptibility as measured at different probing frequencies (1 KHz to 0.5 MHz) for the SrTiO$_3$ doped with (a) Co, (b) Fe, (c) Mn, and (d) Ni on the left, and doped KTaO$_3$ (e) Co, (f) Fe, (g) Mn, and (h) Ni on the right.

FIG. 7. Arrhenius fits (solid lines) to the relaxation peak observed in the doped members of the KTaO$_3$ (top) and SrTiO$_3$ (bottom) series.

In Barrett's equation, at temperatures when $T \gg T_1$, the denominator term $\frac{T_1}{2}$ (coth$\frac{T_1}{2T}$) will asymptotically approach T, and Barrett's equation modifies to the Curie-Weiss law at higher temperatures. On the other hand, when temperature $T \to 0$ K, then the dielectric permittivity varies as $\frac{C}{(\frac{T_1}{2})-T_o}$ or $\frac{2C}{(T_1-2T_o)}$. The positive sign of $(T_1 - 2T_0)$ has been parametrized as a signature of the ferroelectric mode instability due to the quantum fluctuations in some earlier reports on doped quantum paraelectrics [23,24]. The value of $(T_1 - 2T_0)$ deduced from our fitting is positive for all the doped specimens, implying the presence of instability of the ferroelectric mode driven by quantum fluctuations, and it conclusively rules out any possibility of ferroelectricity in these doped systems and further confirms that these doped systems retain their quantum paraelectric behavior down to the lowest measured temperatures. However, the magnitude of $(T_1 - 2T_0)$ as deduced from our fits is seen to vary systematically as a function of the ionic radii of the dopant in the SMT specimens (Table II), indicating that the suppression of quantum fluctuations decreases monotonically as a function of the ionic radii. No such trend is evident in the case of the KMT specimens, presumably due to the fact that the extent
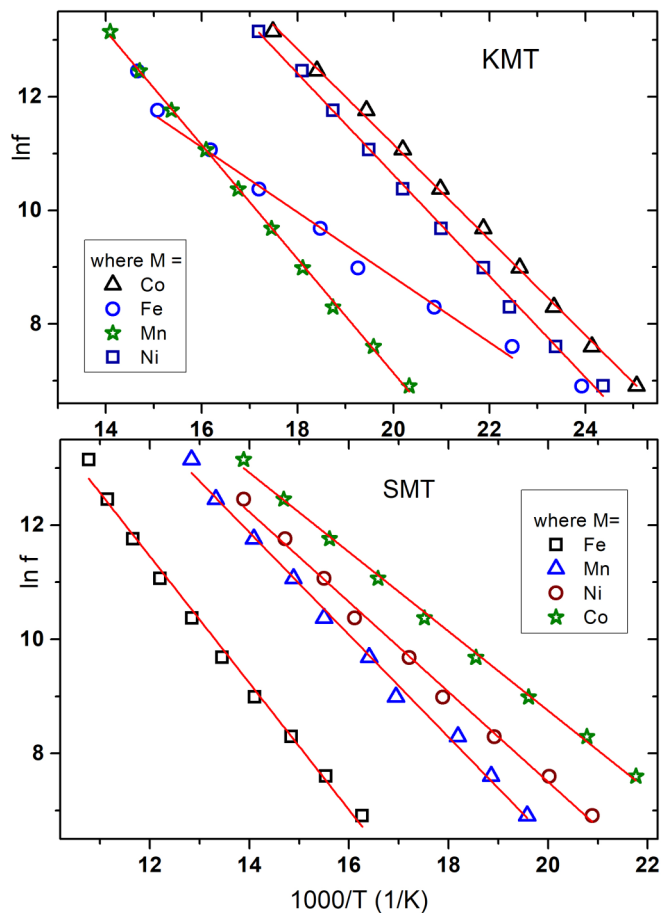
of transition metals that are actually incorporated in the host lattice varies from one transition metal species to another.

In the high-temperature classical regime, the inverse of the dielectric susceptibility would exhibit a Curie-Weiss (T^{-1}) dependence, and a defining feature of the quantum paraelectrics is the crossover to a low-temperature regime where quantum fluctuations dominate. In this regime, the dielectric susceptibility is expected to vary as $1/\epsilon' \propto T^{(d+z-2)/z}$, where d and z refer to the spatial and temporal dimensions, respectively [25]. In the materials under consideration here, $d = 3$ and $z = 1$, resulting in the dielectric susceptibility varying as T^{-2}, as has been observed for both KTaO$_3$ and SrTiO$_3$ below $T \approx 50$ K [25]. Figure 9 depicts the T^2 fit of $1/\epsilon$ for all our doped specimens below 50 K, clearly indicating that doping

TABLE I. The values of the activation energies deduced from the Arrhenius fit to the $\epsilon''(T)$ data.

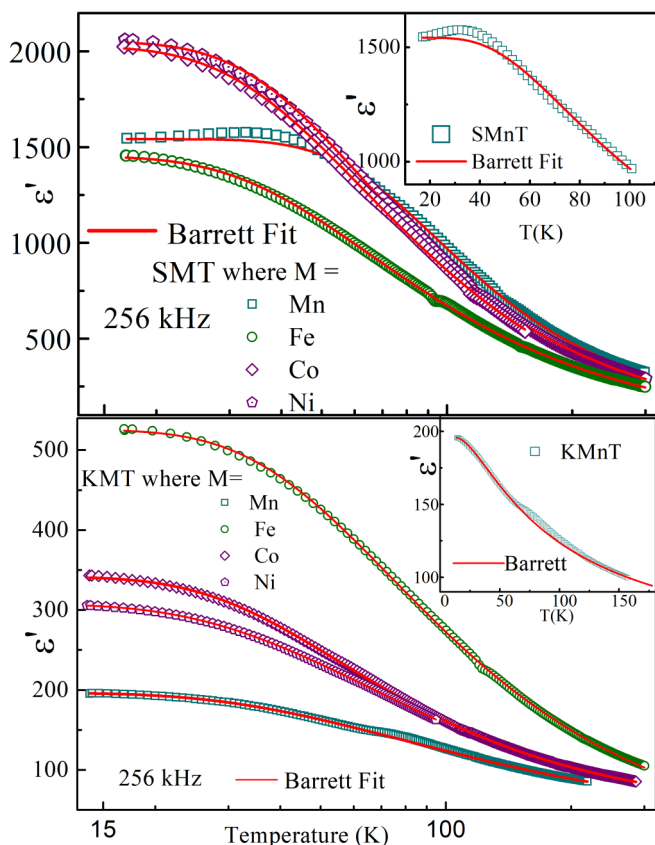| Dopant	SMT (meV)	KMT (meV)
Co	59.35 ± 2.13	73.03 ± 5.40
Ni	69.90 ± 3.11	77.70 ± 4.71
Mn	79.49 ± 2.98	87.29 ± 4.07
Fe	99.95 ± 3.24	51.54 ± 2.84

FIG. 8. The measured $\epsilon'(T)$ for all the doped SrTiO$_3$ (top) and KTaO$_3$ (bottom) specimens. The solid line corresponds to a fit using Barrett's formalism. The insets depict deviations from the fit for the Mn-doped specimens of both the series.
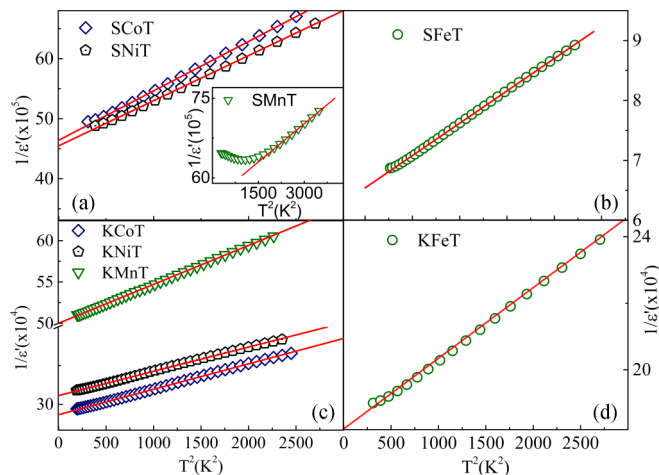

FIG. 9. Inverse permittivity as the function of the square of the temperature of doped systems. Parts (a) and (c) show the SMT and KMT systems doped with Co, Ni, and Mn. Parts (b) and (d) are Fe-doped SMT and KMT, respectively. The solid straight line fitting represents the quantum critical behavior.

of transition metal ions does not cause a significant change in the quantum paraelectric behavior of the host lattices [26], and further rules out the presence of any kind of polar order in these doped materials. We note that the variation in $1/\epsilon$ appears to be smaller than that observed in the undoped STO and KTO specimens [23,27]. This could probably be due to the suppression of the quantum fluctuations as a consequence of doping. We also note that a deviation from this T^2 fit is observed at temperatures as high as 45 K in Mn-doped STO,

TABLE II. Parameters C (Curie constant), T_1 (temperature below which quantum fluctuations overwhelm the thermal ones), T_0 (classical Curie temperature), and $T_1 - 2T_0$ evaluated from fitting of $\epsilon'(T)$ using Barrett's equation for KMT (top) and SMT (bottom) series.

KMT	C	T_1 (K)	T_0 (K)	$T_1 - 2T_0$ (K)
Mn	12699 ± 141	76.3 ± 0.6	-41.5 ± 0.9	159.3 ± 1.9
Fe	31557 ± 86	107.8 ± 0.7	-6.0 ± 0.4	119.8 ± 1.0
Co	12337 ± 90	88.3 ± 0.6	3.0 ± 0.5	94.4 ± 1.2
Ni	21107 ± 50	63.7 ± 0.6	-35.6 ± 1.4	134.9 ± 2.9
SMT	C	T_1 (K)	T_0 (K)	$T_1 - 2T_0$ (K)
Mn	79098 ± 497	203.4 ± 1.8	50.9 ± 1.0	101.5 ± 2.7
Fe	71746 ± 503	103.4 ± 0.3	2.2 ± 0.1	98.5 ± 0.4
Co	81974 ± 937	108.9 ± 1.9	13.7 ± 1.3	81.5 ± 3.2
Ni	82117 ± 349	116.3 ± 0.8	18.1 ± 0.5	80.0 ± 1.3

suggesting that this dopant suppresses quantum fluctuations at a rate that is different from the other transition metals.

The fact that the Mn-doped systems behave a little differently, at least as far as their dielectric properties are concerned, could possibly be due to the fact that the ionic radius of Mn^{+2} is larger than that of the other dopants. In the ATiO$_3$ perovskites, it is known that the A-O framework evokes an interstitial space, which is larger than the size of the body-centered Ti^{+4} ion. For instance, in BaTiO$_3$, a series of ferroelectric phase transitions are encountered upon reducing the temperature, with each of them being associated with a different rattling mode associated with the Ti-O octahedra. On the other hand, when A is replaced by smaller cations such as Ca or Sr, this rattling of Ti is hindered, and hence no ferroelectricity is observed in SrTiO$_3$ and CaTiO$_3$ down to the lowest measured temperatures [28,29]. Increasing quantum fluctuations at low temperatures also helps to stabilize the quantum paraelectric state in these systems. Empirical data suggest that the smaller the size of the A site ion, the larger are the quantum fluctuations, and the higher is the stability of the quantum paraelectric state [30]. Moreover, the critical concentration required to establish a long range or a glassy dipolar state in host quantum paraelectrics also appears to be sensitive to the choice of the dopant. This has already been demonstrated earlier, where 3% Mn doping in KTaO$_3$ was reported to result in a clear signature in the dielectric permittivity, whereas the same amount of Fe doping had no discernible influence [22]. The fact that Mn^{+2} also has the largest number of unpaired electrons among all the doped magnetic transition metal ion configurations could also play a role in influencing the complex interplay between structural considerations and quantum fluctuations in these systems.

C. Magnetism analysis

As described earlier, the presence (or the lack thereof) of a multiglass state in the doped quantum paraelectrics has been contentious due to the possibility that the magnetic spin-

TABLE III. Magnetic transition temperatures corresponding to the different transition metal oxides, which are likely to exist as possible impurities.

Element	Possible oxides	Magnetic transition temperature (K)	Nature of transition
Mn	MnO_2	92	AF
	Mn_3O_4	41–43	Ferri
Ni	NiO	523	AF
	$Ni_2O_3 \cdot H_2O$	525	
Fe	Fe_3O_4	858	Ferri
		120	Verwey
	α Fe_2O_3	260	Morin
		950	AF
Co	Co_3O_4	40	AF

FIG. 11. Temperature dependence of the dc magnetic susceptibility of the doped $KTaO_3$ specimens as measured in the zero-field-cooled and field-cooled protocols at 500 Oe. All these specimens exhibit signatures in the magnetization, which corresponds to the magnetic transitions of one of the magnetic oxides listed in Table III.

glass-like state observed in the Mn-doped $SrTiO_3$ and $KTaO_3$ systems is extrinsic in origin. This is partly due to the fact that a possible impurity oxide (Mn_3O_4) has a magnetic transition in the temperature range of our interest. Moreover, it was also reported that there is no observable scaling between the onset of the magnetic anomaly and the Mn doping level [27,31]. As is also observed in the structural characterization of our specimens, the solubility of magnetic ions in both $SrTiO_3$ and $KTaO_3$ hosts appears to be limited and kinetically hindered, making it imperative that the possibility of a magnetically frozen state is evaluated in these lattices doped with other magnetic transition metal ions. As a reference, Table III lists the magnetic transition temperatures of a number of possible impurity oxides associated with the dopants being used in this study.

Figure 10 depicts the magnetic measurements performed on the SMT series in the zero-field-cooling mode at 1000 Oe. All the specimens (including the Mn-doped one) are observed to be paramagnetic-like, with no trace of any magnetic anomaly associated with long- or short-range magnetic order. This is in clear contradiction to the initial report in which
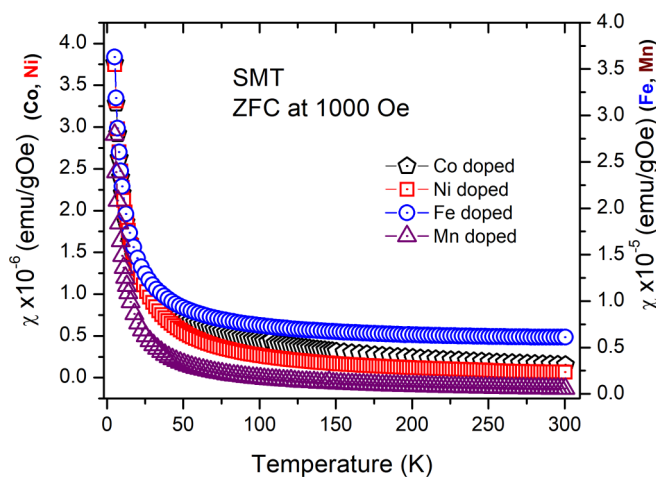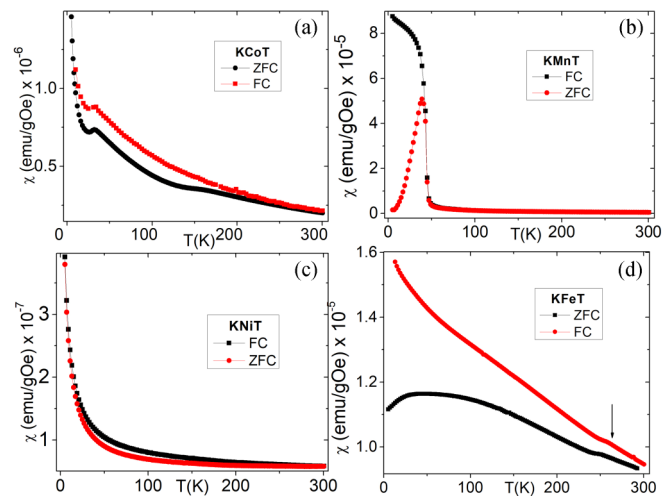

FIG. 10. Temperature dependence of the dc magnetic susceptibility as measured in the doped $SrTiO_3$ systems using the zero-field-cooled protocol. All the specimens appear to be paramagnetic down to the lowest measured temperatures.

Mn-doped $SrTiO_3$ was suggested to be a magnetoelectric multiglass. Our results suggest that most of the Mn have been successfully incorporated into the $SrTiO_3$ lattice, the paramagnetic contribution of which effectively overwhelms the magnetic contribution of the parasitic Mn_3O_4 phase. A similar scenario appears to be valid for all the doped members of this series, as is evident from the fact that none of them exhibit magnetic anomalies in the temperature range of our measurements.

The magnetic measurements of the members of the KMT series as performed in the zero-field-cooled and field-cooled protocols are shown in Fig. 11, and interestingly, all the members of this series exhibit features in the magnetization. Referring to Table III, it is evident that the Co-, Mn-, and Fe-doped specimens exhibit features corresponding to the antiferromagnetic transition of Co_3O_4 [Fig. 11(a)], the ferrimagnetic transition of Mn_3O_4 [Fig. 11(b)], and the Morin transition of α-Fe_2O_3 [Fig. 11(d)], respectively. The Ni-doped specimen [Fig. 11(c)] does not exhibit any feature in the magnetization, probably due to the fact that the magnetic transitions associated with the possible impurities (NiO and Ni_2O_3) lie above the temperature ranges of our measurements. We note that these specimens were observed to be very homogeneous, and traces of impurity phases could be observed only after collecting extensive backscattering images. Though a significant amount of the magnetic dopants appears to have been incorporated into the host lattice, the doped $KTaO_3$ systems do not appear to exhibit any additional feature in the magnetization. Thus our magnetic measurements rule out the possibility of any kind of intrinsic magnetic ordering in the doped members of both the KMT and SMT series. Our observations clearly indicate that the magnetization of these doped specimens could vary drastically as a function of the magnetic dopants incorporated in the host lattice. The measured bulk magnetization thus reflects the competition between the intrinsic paramagnetic-like susceptibility of the

doped $SrTiO_3$ and $KTaO_3$ systems and contributions from remnant impurity oxides of the dopants. The doped quantum paraelectrics clearly remains paramagnetic down to 5 K, and hence any report to the contrary [6–9] is likely to originate from extrinsic effects alone.

IV. CONCLUSION

In summary, we have investigated the doping of magnetic transition metals (Mn, Fe, Ni, or Co) in the quantum para-electrics $SrTiO_3$ and $KTaO_3$ with the aim of verifying the existence (or lack thereof) of coupled magnetic and polar glass states in these systems. Extensive structural and scanning electron microscopy measurements clearly indicate that the magnetic dopants have limited solubility in these host lattices, and traces of spurious impurities are observed even in the most well-processed specimens. Our dielectric measurements show that the doping-induced electrical dipoles exhibit ther-mally activated hopping and appear to be too weakly coupled to exhibit a critical slowing down as is expected from a frozen polar state. Magnetic measurements indicate that all the observed magnetic signatures can be unambiguously at-tributed to the presence of oxides corresponding to the tran-sition metal dopants, and that the doped $SrTiO_3$ and $KTaO_3$ specimens remain paramagnetic down to the lowest measured temperatures. Our results clearly show that the doped quantum paraelectrics do not harbor a multiglass state, at least in the doping concentrations investigated here, and any report to the contrary arises from extrinsic considerations alone. Though the feasibility of concomitant glassy states in the polar and magnetic sectors is an intriguing one—especially due to the possibility of exploring cross-coupled aging and rejuvenation effects—doped quantum paraelectrics are unlikely to offer a testing ground for such an exploration.

[1] M. Fiebig, T. Lottermoser, D. Meier, and M. Trassin, Nat. Rev. Mater. **1**, 16046 (2016).

[2] S.-W. Cheong and M. Mostovoy, Nat. Mater. **6**, 13 (2007).

[3] Y. Tokura, S. Seki, and N. Nagaosa, Rep. Prog. Phys. **77**, 076501 (2014).

[4] W. Kleemann and C. Binek, Multiferroic and magnetoelectric materials, in *Magnetic Nanostructures: Spin Dynamics and Spin Transport*, edited by H. Zabel and M. Farle (Springer, Berlin, 2013), pp. 163–187.

[5] W. Kleemann, P. Borisov, V. V. Shvartsman, and S. Bedanta, EPJ Web Conf. **29**, 00046 (2012).

[6] V. V. Shvartsman, S. Bedanta, P. Borisov, W. Kleemann, A. Tkach, and P. M. Vilarinho, Phys. Rev. Lett. **101**, 165704 (2008).

[7] W. Kleemann, V. V. Shvartsman, S. Bedanta, P. Borisov, A. Tkach, and P. M. Vilarinho, J. Phys.: Condens. Matter **20**, 434216 (2008).

[8] W. Kleemann, S. Bedanta, P. Borisov, V. V. Shvartsman, S. Miga, J. Dec, A. Tkach, and P. M. Vilarinho, Eur. Phys. J. B **71**, 407 (2009).

[9] V. V. Shvartsman, S. Bedanta, P. Borisov, W. Kleemann, A. Tkach, and P. M. Vilarinho, J. Appl. Phys. **107**, 103926 (2010).

[10] D. Choudhury, P. Mandal, R. Mathieu, A. Hazarika, S. Ra-jan, A. Sundaresan, U. V. Waghmare, R. Knut, O. Karis, P. Nordblad, and D. D. Sarma, Phys. Rev. Lett. **108**, 127201 (2012).

[11] K. Singh, A. Maignan, C. Simon, S. Kumar, C. Martin, O. Lebedev, S. Turner, and G. V. Tendeloo, J. Phys.: Condens. Matter **24**, 226002 (2012).

[12] D. Choudhury, S. Mukherjee, P. Mandal, A. Sundaresan, U. V. Waghmare, S. Bhattacharjee, R. Mathieu, P. Lazor, O. Eriksson, B. Sanyal, P. Nordblad, A. Sharma, S. V. Bhat, O. Karis, and D. D. Sarma, Phys. Rev. B **84**, 125124 (2011).

[13] M. Valant, T. Kolodiazhnyi, I. Arčon, F. Aguesse, A.-K. Axelsson, and N. M. Alford, Adv. Funct. Mater. **22**, 2114 (2012).

[14] K. P. Meher, C. Bogicevic, P.-E. Janolin, and K. Varma, J. Solid State Chem. **192**, 296 (2012).

[15] R. Tackett, G. Lawes, B. C. Melot, M. Grossman, E. S. Toberer, and R. Seshadri, Phys. Rev. B **76**, 024409 (2007).

[16] T. Suzuki and T. Katsufuji, Phys. Rev. B **77**, 220402 (2008).

[17] A. I. Lebedev, I. A. Sluchinskaya, A. Erko, and V. F. Kozlovskii, JETP Lett. **89**, 457 (2009).

[18] J. Goldstein, D. E. Newbury, D. C. Joy, C. E. Lyman, P. Echlin, E. Lifshin, S. Linda, and J. R. Michael, *Scanning Electron Microscopy and X-ray Microanalysis* (Springer, New York, 2003).

[19] Z. Trybuła, S. Miga, S. Łoś, M. Trybuła, and J. Dec, Solid State Commun. **209-210**, 23 (2015).

[20] H. Fujishita, S. Kitazawa, M. Saito, R. Ishisaka, H. Okamoto, and T. Yamaguchi, J. Phys. Soc. Jpn. **85**, 074703 (2016).

[21] J. H. Barrett, Phys. Rev. **86**, 118 (1952).

[22] E. L. Venturini, G. A. Samara, V. V. Laguta, M. D. Glinchuk, and I. V. Kondakova, Phys. Rev. B **71**, 094111 (2005).

[23] A. Tkach, P. M. Vilarinho, and A. L. Kholkin, Appl. Phys. Lett. **86**, 172902 (2005).

[24] T. Wei, Y. J. Guo, P. W. Wang, D. P. Yu, K. F. Wang, C. L. Lu, and J.-M. Liu, Appl. Phys. Lett. **92**, 172912 (2008).

[25] S. E. Rowley, L. J. Spalek, R. P. Smith, M. P. M. Dean, M. Itoh, J. F. Scott, G. G. Lonzarich, and S. S. Saxena, Nat. Phys. **10**, 367 (2014).

[26] P. Chandra, G. G. Lonzarich, S. E. Rowley, and J. F. Scott, Rep. Prog. Phys. **80**, 112502 (2017).

[27] M. Valant, T. Kolodiazhnyi, A.-K. Axelsson, G. S. Babu, and N. M. Alford, Chem. Mater. **22**, 1952 (2010).

[28] C. Ménoret, J. M. Kiat, B. Dkhil, M. Dunlop, H. Dammak, and O. Hernandez, Phys. Rev. B **65**, 224104 (2002).

[29] U. Aschauer and N. A. Spaldin, J. Phys.: Condens. Matter **26**, 122203 (2014).

[30] M. E. Lines and A. M. Glass, *Principles and Applications of Ferroelectrics and Related Materials* (Oxford University Press, Oxford, 1977).

[31] R. O. Kuzian, V. V. Laguta, A.-M. Daré, I. V. Kondakova, M. Marysko, L. Raymond, E. P. Garmash, V. N. Pavlikov, A. Tkach, P. M. Vilarinho, and R. Hayn, Europhys. Lett. **92**, 17007 (2010).